On the Fluxional Behavior of Monocoordinated Diimines and Azines

Santiago Alvarez,* Maria-Jose Bermejo, and Jordi Vinaixa*

Contribution from the Department de Quimica Inorganica, Facultat de Quimica, Universitat de Barcelona, 08028 Barcelona, Spain. *Received December 1, 1986*

Abstract: Intramolecular mechanisms for the haptotropic shift of transition-metal centers in monocoordinate complexes with potentially bidentate diimines and azines have been analyzed by means of qualitative molecular orbital studies, and the factors controlling the height of the barriers for such shifts are discussed. Related processes are the tautomerism in protonated formamidinates or triazenides, as well as the haptotropic shifts in main group metal complexes. A common feature for all these systems is the loss of overlap between the acceptor orbital and the diimine's lone pairs along the reaction path, while a unique feature of the transition-metal complexes is the appearance of a four-electron repulsion between the lone pairs and one of the metal's "t_{2g}" orbitals. For octahedral complexes, the height of the potential energy barrier is expected to be in the order Cr < Mn < Fe > Co, and the presence of a π-acceptor ligand in the trans position is expected to lower the barrier. On the ligand side, the nitrogen–nitrogen separation and the lone pair orientation are the main factors determining the height of the barrier, while mixing with orbitals of the intervening carbon skeleton accounts for smaller changes in the barrier. According to the orbital analysis presented, redox reactions should allow interconversion of monodentate and bidentate compounds, while irradiation with light of a wavelength corresponding to a ligand field transition should produce an important lowering of the barrier for the fluxional process.

There is a rich chemistry related to the coordination of chelating diimines to transition-metal centers. This class of ligands is characterized by the presence of two equivalent donor nitrogen atoms with an sp^2 hybridization; some of the most common ones, as well as the related azines, are represented in Chart I. Bipyridine and phenanthroline typically form well-known chelates,[1] but even ligands with smaller bites, such as naphthyridine or triazenido, form chelates.[2] There is also a family of dinuclear and polynuclear complexes in which a diimine acts as bridging ligand,[2m,3] and finally there are a number of compounds in which a diimine or an azine is monocoordinated through one of its nitrogen atoms[2m,4,5] in an octahedral complex. When the ligand is linked to a square-planar[6] or a linear[7] transition-metal fragment the second nitrogen may weakly interact with the metal as in Chart

Chart I

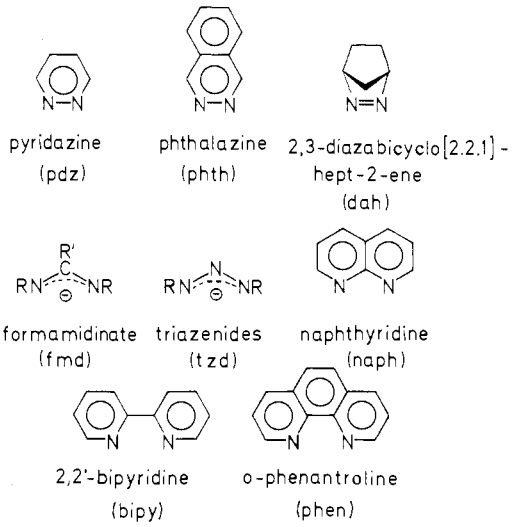

Chart II

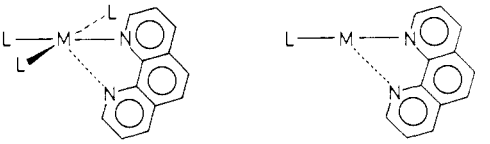

Table I. Metal–Nitrogen Bond Distances in Square-Planar and Linear Complexes

compound	$M-N_1$	$M-N_2$	Δd	ref
$[AuBr_3(Me_2phen)]$	2.08 (2)	2.61 (2)	0.53	6c
$[AuCl_3(Me_2phen)]$	2.09 (1)	2.58 (1)	0.49	6c
$[CuCl_2(Me_2naph)_2]$	1.98 (1)	2.80	0.82	6i
cis-$[PtCl(PEt_3)_2(phth)]^+$	2.08 (3)	2.97 (3)	0.89	6b
cis-$[PtCl(PEt_3)_2(naph)]^+$	2.08 (1)	3.05 (1)	0.97	6e
cis-$[PtCl(PEt_3)_2(phen)]^+$	2.14 (2)	2.84 (2)	0.70	6a
$Ni(C_6F_5)(dppe)(Me_2naph)]^+$	1.98 (1)	2.72 (1)	0.74	8a
$[Pd(PPh_3)_2Cl(tzd)]$	2.033 (5)	2.836 (5)	0.803	9
$[Pt(PPh_3)_2H(tzd)]$	2.09 (2)	2.91 (2)	0.82	9
$[Pt(PPh_3)_2Cl(tzd)]$	2.11 (2)	3.01 (2)	0.90	9
$[Hg_2(naph)_2]^{2+}$	2.03 (3)	2.78 (1)	0.75	7b
$[Hg_2(phen)(NO_3)_2]$	2.30	2.48	0.18	7c

(1) (a) Serpone, N.; Ponterini,G.; Jameison, M. A.; Bolletta, F.; Maestri, M. *Coord. Chem. Rev.* **1983**, *50*, 209. (b) Constable, E. C. *Polyhedron* **1983**, *2*, 551. (c) Gillard, R. D. *Coord. Chem. Rev.* **1975**, *16*, 67.

(2) (a) Clearfield, A.; Gopal, R.; Olsen, R. W. *Inorg. Chem.* **1977**, *16*, 911. (b) Wagner, J. R.; Hendricker, D. G. *J. Inorg. Nucl. Chem.* **1975**, *37*, 1375. (c) Hendricker, D. G.; Bodner, R. L. *Inorg. Chem.* **1970**, *9*, 273. (d) Hendricker, D. G. *Inorg. Chem.* **1969**, *8*, 2328. (e) Bodner, R. L.; Hendricker, D. G. *Inorg. Chem.* **1970**, *9*, 1255. (f) Foster, R. J.; Hendricker, D. G. *Inorg. Chim. Acta* **1972**, *6*, 371. (g) Bodner, R. L.; Hendricker, D. G. *Inorg. Chem.* **1973**, *12*, 33. (h) Hendricker, D. G.; Reed, T. E. *Inorg. Chem.* **1969**, *8*, 685. (i) Emad, A.; Emerson, K. *Inorg. Chem.* **1972**, *11*, 2288. (j) Cavanaugh, M. A.; Cappo, V. M.; Alexander, C. J.; Good, M. L. *Inorg. Chem.* **1976**, *15*, 2615. (k) Foster, R. J.; Hendricker, G. D. *J. Inorg. Nucl. Chem.* **1972**, *4*, 3795. (l) Brown, L. D.; Ibers, J. A. *Inorg. Chem.* **1976**, *15*, 2788. (m) Paudler, W. W.; Sheets, R. M. *Adv. Heterocycl. Chem.* **1983**, *33*, 147.

(3) (a) Sacconi, L.; Mealli, C.; Gatteschi, D. *Inorg. Chem.* **1974**, *13*, 1985. (b) Gatteschi, D.; Mealli, C.; Sacconi, L. *Inorg. Chem.* **1976**, *15*, 2774. (c) Mealli, C.; Zanobini, F. *J. Chem. Soc., Chem. Commun.* **1982**, 97. (d) Tiripicchio, A.; Tiripicchio-Camellini, M.; Usón, R.; Oro, L. A.; Ciriano, M. A.; Viguri, F. *J. Chem. Soc., Dalton Trans.* **1984**, 125. (e) Cotton, F. A.; Hanson, B. E.; Jameson, J. D.; Stuls, B. R. *J. Am. Chem. Soc.* **1977**, *99*, 3293. (f) Ploeg, A. F. M. J. van der; Koten, G. van; Vrieze, K. *J. Organomet. Chem.* **1982**, *226*, 93. (g) Ploeg, A. F. M. J. van der; Koter, G. van; Vrieze, K.; Spek, A. L.; Duisenberg, A. J. M. *Organometallics* **1982**, *1*, 1066. (h) Beck, J.; Strähle, J. *Angew. Chem., Int. Ed. Engl.* **1986**, *25*, 95. (i) Corbett, M.; Hoskins, B. F.; McLeod, M. J.; O'Day, B. P. *Aust. J. Chem.* **1975**, *28*, 2377. (j) O'Connor, J. E.; Jannsonis, G. A.; Corey, E. R. *J. Chem. Soc., Chem. Commun.* **1968**, 445. (k) Brown, I. D.; Dunitz, J. D. *Acta Crystallogr.* **1961**, *14*, 480. (l) Beck, J.; Strähle, J. *Z. Naturforsch.* **1986**, *41b*, 4. (m) Beck, J.; Strähle, J. *Angew. Chem., Int. Ed. Engl.* **1985**, *24*, 409. (n) Beck, J.; Strähle, J. *Acta Crystallogr. C*, submitted for publication.

(4) (a) Dixon, K. R.; Eadie, D. T.; Stobart, S. R. *Inorg. Chem.* **1982**, *21*, 4318. (b) Heberhold, M.; Leonhard, K.; Kreiter, C. G. *Chem. Ber.* **1974**, *107*, 3222. (c) Eaton, S. S.; Eaton, G. R.; Holm, R. H. *J. Organomet. Chem.* **1972**, *39*, 179.

(5) (a) Grove, D. M.; Koten, G. van; Ubbels, H. J. C.; Vrieze, K.; Niemann, L. C.; Stam, C. H. *J. Chem. Soc., Dalton Trans.* **1986**, 717. (b) Bombieri, G.; Immirzi, A.; Tomiolo, L. *Inorg. Chem.* **1976**, *15*, 2428. (c) Immirzi, A.; Porzio, W.; Bombieri, G.; Tomiolo, L. *J. Chem. Soc., Dalton Trans.* **1980**, 1098. (d) Laing, K. R.; Robinson, S. D.; Uttley, M. F. *J. Chem. Soc., Dalton Trans.* **1974**, 1205. (e) Robinson, S. D.; Utley, M. F. *J. Chem. Soc. D* **1971**, 1315. (f) Tomiolo, L.; Immirzi, A.; Croatto, U.; Bombieri, G. *Inorg. Chim. Acta* **1976**, *19*, 209. (g) Bradley, W.; Wright, I. *J. Chem. Soc.* **1956**, 640.

0002-7863/87/1509-5316$01.50/0

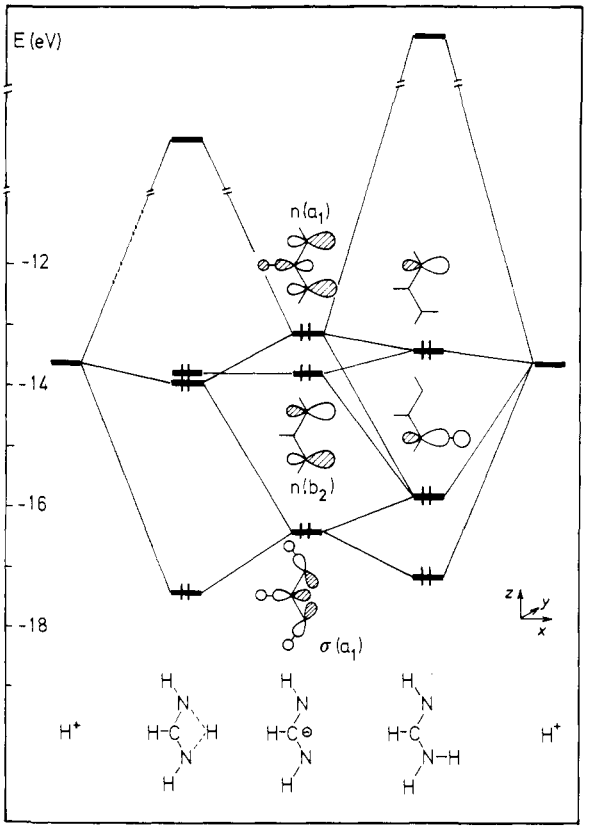

Figure 1. Interaction diagram of a formamidinate ionwith a proton in "monodentate" (right) and "bidentate" (left) coordination modes.

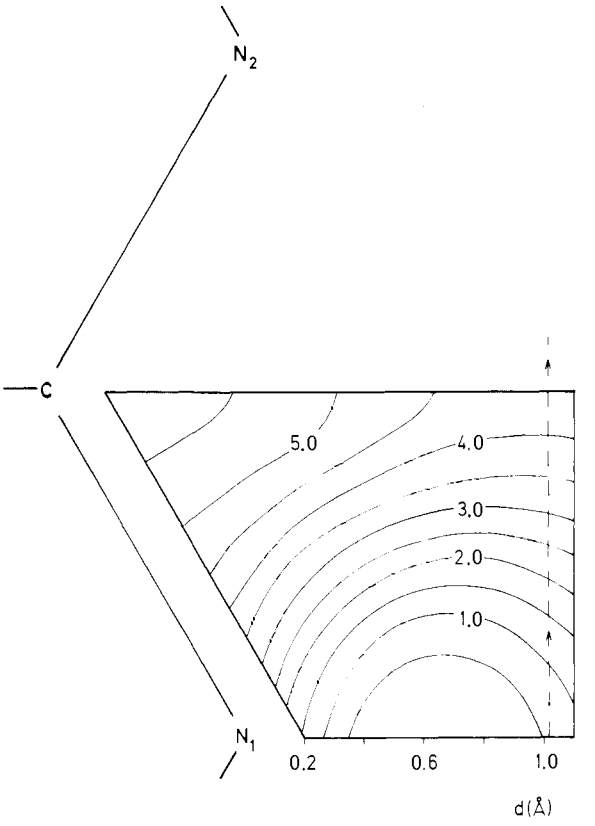

Figure 2. Potential energy surface for the haptotropic shift of a proton in a formamidinate ion. The upper part of the surface (not shown) is symmetric to the lower one. Equipotential lines are separated by 0.5 eV.

II. The two nitrogen–metal distances are clearly different in those cases (Table I). The shortest distance to the second nitrogen atom corresponds to a phenanthroline derivative.

In some cases, the monodentate ligands have been shown to exchange the coordination position, in what could be called a haptotropic shift.[10] The experimental activation energies found for those processes are collected in Table II. If we could establish the factors that determine the height of the barrier for these fluxional processes, one would probably be able to make some predictions and suggest new experiments. We wish to examine in particular the effects of an isoelectronic substitution of the transition-metal ion, the differences among several ligands, and the possibilities for some chemical transformations.

Scheme I

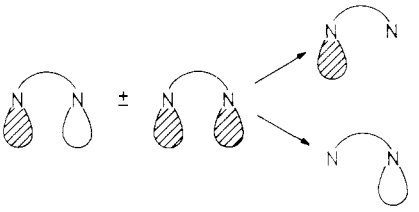

The Orbital Interaction of Potentially Bidentate Ligands with a Proton

The organic counterpart for these dynamic processes can be obtained if a proton is substituted for the isolobal transition-metal fragments, and this is usually referred to as tautomerism. These processes are experimentally known for the formamidinates and triazenides[14] as well as for naphthyridine.[15] We will study one of these cases first, the tautomerism of the protonated formamidinate (fmd, R = R′ = H, Chart I), because it can be analyzed in terms of σ orbitals only. Later on, we will see that the fluxional process in transition-metal compounds presents the same qualitative features in the σ system and is only slightly complicated due to the presence of π-type interactions.

The molecular orbitals of fmd (Figure 1) can be classified according to their representation in the C_{2v} point group. Therefore, the σ and π orbitals do not mix and can be separately discussed. The π orbitals are much like those of a typical allylic system and will not be commented here[16] but, at difference with an allyl anion,

(6) (a) Bushnell, G. W.; Dixon, K. R.; Khan, M. A. *Can. J. Chem.* **1974**, *52*, 1367. (b) Bushnell, G. W.; Dixon, K. R. *Can. J. Chem.* **1978**, *56*, 878. (c) Robinson, W. T.; Sinn, E. *J. Chem. Soc., Dalton Trans.* **1975**, 726. (d) Balch, A. L.; Cooper, R. D. *J. Organomet. Chem.* **1979**, *169*, 97. (e) Bushnell, G. W.; Dixon, K. R.; Khan, M. A. *Can. J. Chem.* **1978**, *56*, 450. (f) Dixon, K. R. *Inorg. Chem.* **1977**, *16*, 2618. (g) Brandon, J. B.; Collins, M.; Dixon, K. R. *Can. J. Chem.* **1978**, *56*, 950. (h) Schmidbaur, H.; Dash, K. D. *J. Am. Chem. Soc.* **1973**, *95*, 4855. (i) Mealli, C.; Sacconi, L. *Acta Crystallogr.* **1977**, *B33*, 713. (j) Vicente, J.; Chicote, M. T.; Bermúdez, M. D.; Jones, P. G.; Fittschen, C.; Sheldrick, G. M. *J. Chem. Soc., Dalton Trans.* **1986**, 2361. (k) Marangon, G.; Pitteri, B.; Bertolasi, V.; Gilli, G.; Ferretti, V. *J. Chem. Soc., Dalton Trans.* **1986**, 1941.

(7) (a) Singh, P.; Clearfield, A.; Bernal, I. *J. Coord. Chem.* **1971**, *1*, 29. (b) Dewan, J. C.; Kepert, D. L.; White, A. H. *J. Chem. Soc., Dalton Trans.* **1975**, 490. (c) Elder, R. C.; Halpern, J.; Pond, J. S. *J. Am. Chem. Soc.* **1967**, *89*, 6877.

(8) (a) Bermejo, M. J.; Nowell, I. W.; Pidcock, A.; Vinaixa, J., to be published. (b) Ruiz, J. I.; Vinaixa, J., to be published. (c) Bermejo, M. J.; Martínez, B.; Vinaixa, J. *J. Organomet. Chem.* **1986**, *304*, 207. (d) Bermejo, M. J.; Vinaixa, J., to be published. (e) Bermejo, M. J.; Ruiz, J. I.; Vinaixa, J. *Transition Met. Chem.*, in press.

(9) Toniolo, L.; Immirzi, A.; Croatto, U.; Bombieri, G. *Inorg. Chim. Acta* **1976**, *19*, 209.

(10) Although commonly used in organometallic chemistry to describe fluxional processes of metal–polyene complexes, the term "haptotropic rearrangement" describes in general the change in connectivity (hapto number) of a metal to a ligand with multicoordinate site possibilities: Anh, N. T.; Elian, M.; Hoffmann, R. *J. Am. Chem. Soc.* **1978**, *100*, 110. Albright, T. A.; Hofmann, P.; Hoffmann, R.; Lillya, C. P.; Dobosh, P. A. *J. Am. Chem. Soc.* **1983**, *105*, 3396.

(11) Schmidbaur, H.; Wolfsberger, W. *Angew. Chem., Int. Ed. Engl.* **1967**, *6*, 448.

(12) Schmidbaur, H. *Forsch. Chem. Forsch.* **1969**, *13*, 167.

(13) Calder, I. C.; Garratt, P. J. *J. Chem. Soc. B* **1967**, 660.

(14) Roberts, R. M. *J. Am. Chem. Soc.* **1950**, *72*, 3608.

(15) Bacci, M.; Dei, A.; Morassi, R. *Inorg. Chim. Acta* **1973**, *7*, 209.

Table II. Experimental and Calculated Barriers for the Haptotropic Shift of Monocoordinated Diimines and Azines

compound[a]	exptl barrier (kcal/mol)	ref	compound	calcd barrier (kcal/mol)
		Octahedral Complexes		
$[Cr(CO)_5(phth)]$	21.5	4a	$[CrH_5(pdz)]^{5-}$	16
$[Mn(CO)_5(pdz)]^+$	$\gg 17^d$	8e	$[MnH_5(pdz)]^{4-}$	39
$[Fe(CO)_2Cp(pdz)]^+$	$\gg 16^d$	8c	$[FeH_5(pdz)]^{3-}$	65
$[W(CO)_5(phth)]$	18.4	4a		
$[Ru(i\text{-}Pr\text{-}TPP)(CO)(Me_2pdz)]$	12.1–15.1[b]	4c		
$[Cr(aryl)(CO)_2(dah)]$	17.0–19.8	4b	$[CrH_5(pdz)]^{5-}$	16
$[Cr(CO)_5(naph)]$	13.0	4a	$[CrH_5(naph)]^{5-}$	6
$[Mn(phen)(CO)_3(naph)]^+$	15.3[e]	8b	$[MnH_5(naph)]^{4-}$	31
$[Fe(CO)_2Cp(naph)]^+$	$\gg 17.0$[e,d]	8c	$[FeH_5(naph)]^{3-}$	52
			$[CoH_5(naph)]^{2-}$	47
$[W(CO)_5(naph)]$	14.1	4a		
		Square-Planar Complexes		
trans-$[Pd(PPh_3)_2Cl(R_2fmd)]$	16.3[c]	9		
cis-$[Pt(PPh_3)_2Cl(R_2fmd)]$	16.1[c]	9	*cis*-$[Pt(PH_3)_2Cl(fmd)]$	23
trans-$[Pd(PPh_3)_2Cl(R_2tzd)]$	13.9[c]	9		
cis-$[Pt(PPh_3)_2Cl(R_2tzd)]$	13.7[c]	9	*cis*-$[Pt(PH_3)_2Cl(tzd)]$	20
cis-$[Pt(PR_3)_2Cl(pdz)]^+$	17.0[e]	6f	*cis*-$[Pt(PH_3)_2Cl(pdz)]^+$	26
cis-$[Pt(PEt_3)_2Cl(phth)]^+$	18.2[e]	6f	*cis*-$[Pt(PH_3)_2Cl(pdz)]^+$	26
cis-$[Pt(PR_3)_2Cl(naph)]^+$	12.2[e]	6f	*cis*-$[Pt(PH_3)_2Cl(naph)]^+$	22
cis-$[Pt(PR_3)_2Cl(phen)]^+$	9.6[e]	6f		
$[AuX(Me)_2(Me_2naph)]$	10.1–10.6[e]	6h		
$[NiR(dppe)(pdz)]^+$	12.6–13.7[e]	8d	$[Ni(PH_3)_2Cl(pdz)]^+$	29
		Non-Transition Metals		
$Me_3Ga[Me_2Si(NPMe_3)_2]$	12.8	11		
$Me_3Al[Me_2Si(NPMe_3)_2]$	13.4	11		
$R_3Ge[R_2P(NSiR_3)_2]$	≈15.0	12		
			$AlH_3(pdz)$	7
			$AlH_3(naph)$	7

[a] *i*-Pr-TPP = tetra(*p*-isopropylphenyl)porphinato; dppe = bis(diphenylphosphino)ethane. [b] Values for different positions of the methyl substituents or different solvents. [c] Values calculated from the reported NMR according to ref 13. [d] The signals from which $\Delta G^{\ddagger}$ is calculated, according to ref 13, are well separated at the highest studied temperature. The value given in the table is therefore a lower limit for $\Delta G^{\ddagger}$. [e] Experimental barrier given as the increase in free energy. It can be compared to the calculated enthalpy difference since the entropic contribution at $T \approx 300$ K has been found to be very small.[4a]

two σ orbitals are replaced by two nonbonding orbitals $n(a_1)$ and $n(b_2)$, which are the symmetric and antisymmetric combinations of the nitrogens' lone pairs. Notice that one of the C–H σ bonding molecular orbitals, $\sigma(a_1)$, has a large density in the lone pairs region as well and can therefore act as a donor orbital also.

If we let fmd interact with H^+ through only one nitrogen atom, the symmetry is lowered to C_s and all the lone pair orbitals can mix. This is done, as shown in Scheme I, in order to localize a lobe on one nitrogen to form a σ bond with the proton and another lobe on the other nitrogen to hold a nonbonding lone pair. Additionally, $\sigma(a_1)$ is stabilized due to mixing with the bonding MO.

The next step is to define a reasonable path for the migration of the proton from one nitrogen to the other one. A potential energy surface for a migration in the plane of fmd is shown in Figure 2. The minimum energy path is approximately a straight line parallel to the N—N vector and the resulting calculated barrier is about 4 eV. Although the energy values obtained from an Extended Hückel calculation might be misleading, in this case the qualitative features of the energy surface can be attributed to fundamental reasons such as symmetry and overlap. Hence, we will continue our analysis using the path marked with a dashed line in Figure 2, with a N–H distance of 1.03 Å, more realistic than the calculated minimum which is a little too short due to the exclusion of internuclear repulsions in the effective hamiltonian employed.

The evolution of the overlap of the proton 1s orbital with the fmd orbitals (Figure 3, upper part) along the reaction path can be understood from the topology of the lone pair orbitals of fmd (Figure 1). The decreased overlap of 1s with the p_x orbital of N_1 along the reaction path is compensated in part by an increase in its overlap with p_x of N_2 (Figure 3, lower part). The small

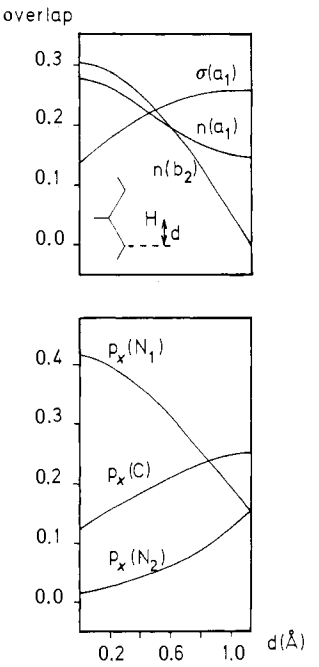

Figure 3. Overlap integrals of the H 1s orbital with the molecular orbitals of a formamidinate ion (above) and with the atomic orbitals of its constituent atoms (below) along the path marked with a dashed line in Figure 2.

negative contribution of $p_x(C)$ to $n(a_1)$ somewhat decreases the overall $1s/n(a_1)$ overlap at the top of the barrier. The overlap of 1s with $n(b_2)$, on the other hand, drops to zero along the reaction path as imposed by the symmetry mismatch when the proton reaches the central position.

(16) For the description of the π molecular orbitals of allylic systems see, e.g.: Jorgensen, W. L.; Salem, L. *The Organic Chemist's Book of Orbitals*; Academic Press: New York, 1973. Lowe, J. P. *Quantum Chemistry*; Academic Press: New York, 1978.

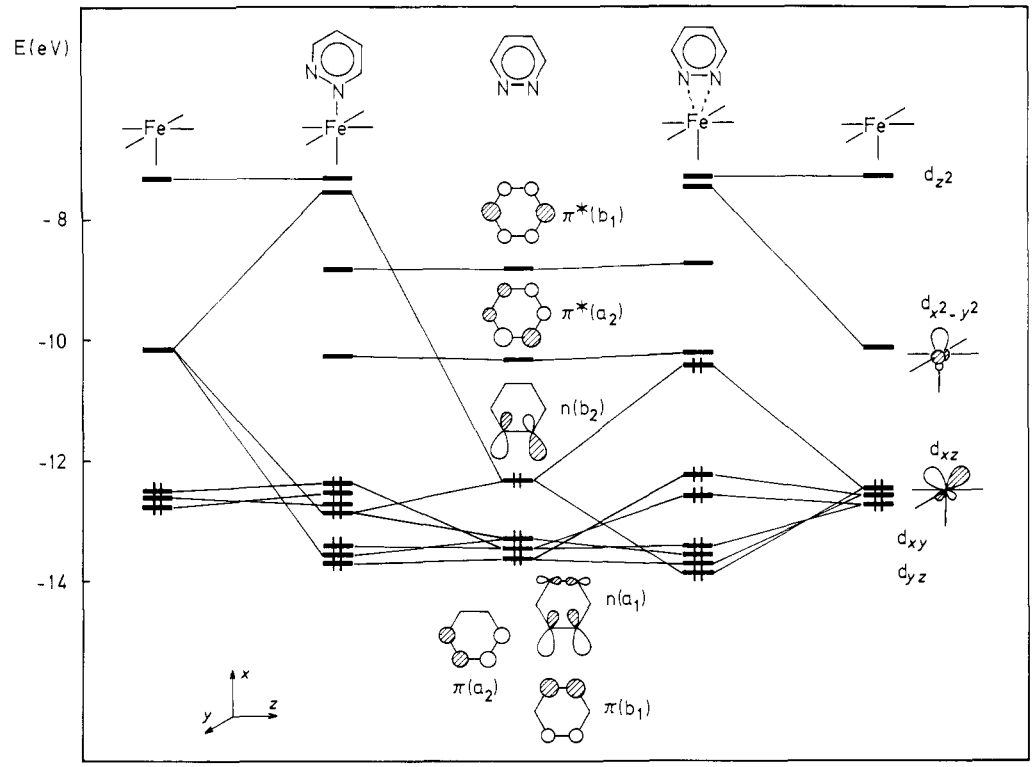

Figure 4. Interaction diagram of pyridazine with a d^6-ML_5 fragment in monodentate (left) and bidentate (right) coordination modes, using FeH_5^{3-} as a model.

At the transition state the proton is still bound and the required activation energy is smaller than the dissociation energy (calculated value: 6.3 eV), indicating that the tautomeric process is likely to be intramolecular. The anihilation of the overlap of 1s with $n(b_2)$ cannot be avoided since it is imposed by symmetry. The overlap with $n(a_1)$ in the transition state can be tuned by adequate substitutions: Adding an electronegative substituent to the carbon atom decreases its contribution to $n(a_1)$, increasing the overlap and slightly decreasing the barrier (by 0.1 eV in calculations with F as substituent); substitution of a nitrogen for the carbon atom works in the same direction but the effect is larger, the barrier being lowered by 0.3 eV. Experimental values for these barriers have not been reported, but for transition-metal compounds with the same ligands, the same trend is experimentally found as discussed below.

Octahedral ML_5 Fragments

In order to analyze the fluxional process for a transition metal with its π orbitals, we rather choose pyridazine (pdz) as the switching ligand for which there is no intervening atom between both donor nitrogens, thus simplifying the analysis of the σ interactions.

The interaction diagram of a pyridazine ligand with an ML_5 group[17] in both the monodentate and the bidentate coordination modes is presented in Figure 4. The fragment orbitals of an ML_5 group are well-known,[18] and its a_1, and b_2 orbitals can be recognized in Figure 4: they are labeled $d_{x^2-y^2}$ and d_{xz}, respectively. For a d^6 configuration $d_{x^2-y^2}$ is empty and d_{xz} is occupied. The pyridazine valence orbitals are presented in the central part of Figure 4. The occupied orbitals shown are the two combinations of the nitrogen lone pairs, $n(a_1)$ and $n(b_2)$, and two π orbitals of symmetry a_2 and b_1. $n(a_1)$ is clearly lower in energy than $n(b_2)$, not only because of its N–N π-bonding character but also due to its mixing with the C_4–C_5 σ-bonding orbital. Higher in energy are two additional π orbitals of a_2 and b_1 symmetry. The nature and approximate position of the highest occupied molecular orbitals agree well with the photoelectron spectrum of pyridazine,[19] where the lower ionization potential (−8.71 eV), corresponding to a nonbonding orbital is followed by three bands close in energy (one at −10.48 and two overlapping bands at ca. −11.1 eV), assigned to one nonbonding and two π-bonding orbitals.

The description of the interaction diagram (Figure 4, left) is straightforward. In the monodentate situation for $FeL_5(pdz)$, going from lower to higher energies, one finds first the two n and the two π orbitals of pdz commented on above. Both $n(a_1)$ and $n(b_2)$ interact with $d_{x^2-y^2}$ forming a M–N σ-bonding MO, mostly localized on one nitrogen atom, and a lone pair primarily localized on the uncoordinated nitrogen, as happens in the formamidinate discussed above. Then the t_{2g}-like set of d orbitals is found. All these orbitals are occupied for a d^6 ion. It is important to notice at this point that interaction of d_{xz} with either of the lone pairs is negligible: one of the sp^2 lobes is orthogonal to d_{xz}, and the other is too far away to overlap. The two lowest empty orbitals turn out to be π^* of pyridazine; a little higher appear d_{z^2} and $d_{x^2-y^2}$, reminiscent of the e_g set of an octahedral ligand field. One might expect the inverse ordering: pyridazine-π^* above the e_g set, and we shall be careful enough not to draw any conclusions which could depend on that relative ordering.

Some changes appear in the interaction diagram (Figure 4, right) for the bidentate situation. The interaction of the lone pair orbitals with $d_{x^2-y^2}$ is somewhat weaker than that for the monodentate case; the difference is not large because of the short M–N distances chosen for the intermediate. For a more accurate evaluation of the geometry at the transition state, the reader is referred to the work of Kang, Albright, and Mealli.[20] On the other hand, the occupied d_{xz} interacts with the occupied $n(b_2)$, giving rise to a four-electron repulsion. Therefore, the system is destabilized with respect to monodentate coordination, resulting in a barrier in the way to the alternative monocoordination. Note

(17) The $Fe^{II}L_5$ fragment has been replaced in our calculations by a FeH_5^{3-} model. Test calculations were also carried out on the real compound $[Fe(Cp)(CO)_2]^+$, and the results were essentially the same as far as the present discussion is concerned.

(18) For a general description of the orbitals of an ML_5 fragment, see: Albright, T. A.; Burdett, J. K.; Whangbo, M.-H. *Orbital Interactions in Chemistry*; J. Wiley: New York, 1985. Albright, T. A. *Tetrahedron* **1982**, *38*, 1339.

(19) Åsbrink, L.; Fridh, C.; Jonsson, B. Ö.; Lindholm, E. *Int. J. Mass Spectrom. Ion Phys.* **1972**, *8*, 229.

(20) Kang, S.-K.; Albright, T. A.; Mealli, C., submitted for publication.

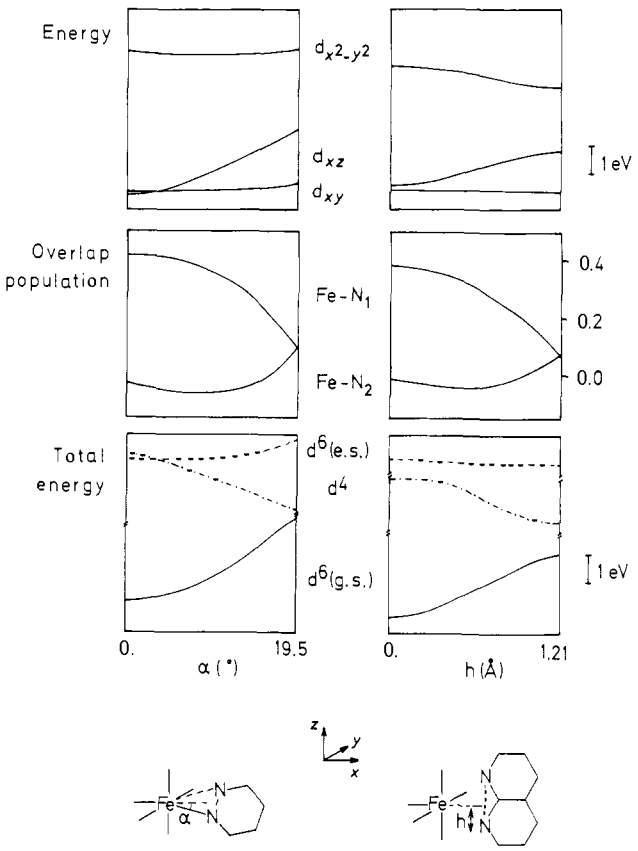

Figure 5. Simplified Walsh diagram (above), atomic overlap populations (middle), and total energies (bottom) for the haptotropic shift of an FeH_5^{3-} fragment on pyridazine (left) and naphthyridine (right). In the total energy diagram, the solid line corresponds to the ground state of a d^6 ML_5 fragment, the dashed line to a ligand field excited state, and the dot-dashed line to the ground state of a d^4 ML_5 fragment.

that for systems with two less electrons (i.e., a d^6 ML_4 or a d^4 ML_5 fragment) the antibonding combination of the b_2 orbitals would be empty and the chelate would be more stable than the monodentate complex.

A third, smaller contribution to the barrier arises from interaction of the metal orbitals with the π orbitals of pyridazine. In the bidentate case the interaction of d_{xy} with $\pi(b_1)$ of pdz is a four electron–two orbital destabilizing one. In the monodentate case, d_{xy} can also mix with the empty $\pi^*(a_2)$, making this interaction a bonding one. The different π interaction in the mono- and bidentate cases can be seen in the position of the d_{xy} orbital in Figure 4.

Some aspects of the haptotropic shift are best illustrated with a Walsh diagram. The chosen reaction path is one in which sliding and rotation of the ligand are combined in such a way as to make the M–N distances in the bidentate intermediate equal to the bonding distance in the monodentate case (Figure 5). In the Walsh diagram, only those orbitals whose energies vary significantly along the reaction path are shown. The HOMO (d_{xz}), nonbonding in the monodentate situation, is made antibonding in the bidentate case through interaction with $n(b_2)$; the probability contour plots of this orbital (Figure 6, lower part) show its nonbonding and antibonding nature at the monodentate and bidentate positions, respectively. Through interaction with the ligand's lone pair orbitals, $d_{x^2-y^2}$ becomes the Fe–N σ-antibonding MO; its decrease in energy along the reaction path is an artifact of the geometry chosen for the transition state as commented above, but there is an additional factor keeping $d_{x^2-y^2}$ highly antibonding in the early stages of the shift. In fact, little symmetry is preserved along the reaction path, and only the plane of the sliding ligand is a symmetry plane; both $d_{x^2-y^2}$ and d_{xz} are symmetric with respect to that plane and they are allowed to mix. The mixing of these two orbitals can be seen as a rehybridization which provides $d_{x^2-y^2}$ with the optimum orientation to overlap with the lone pair orbital

Chart III

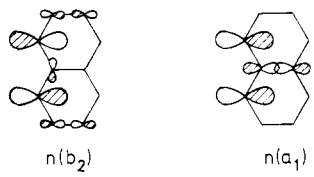

of the closest nitrogen atom, and at the same time d_{xz} is reoriented away from the same ligand orbital. These reorientations show up in the contour plots of both d orbitals (pdz case, Figure 6). The third line in our simplified Walsh diagram corresponds to the d_{xy} orbital; its interaction with the π system of the ligand varies little along the shift and contributes very little to the activation energy.

According to the above discussion, the overall metal–ligand bonding decreases along the reaction path. However, the fact that some Fe–N_2 bonding is being built up simultaneously to the Fe–N_1 bond weakening implies that the bidentate intermediate is still bound, as indicated by the positive overlap populations in Figure 5. This result suggests that the haptotropic shift is likely to be intramolecular for the studied case. A comparison of the computed barriers with bond dissociation energies for similar systems at both the EH and SCF levels can be found in the paper by Kang, Albright, and Mealli.[20]

Two features appear clearly in the total one-electron energy curves of Figure 5. The bond weakening and the four-electron repulsions produce a barrier for the haptotropic shift (calculated values for model compounds are presented in Table II), while for a compound with two less electrons the minimum is located at the bidentate structure. Consequently, one could expect chemical or electrochemical two-electron oxidation reactions to convert a monodentate complex into a chelate and reduction reactions to generate monodentate species from bidentate ones, a synthetic route which might be worth exploring. On the other hand, a ligand field excitation $d_{xz} \rightarrow d_{x^2-y^2}$ almost supresses the barrier for the shift. Perhaps one would be able to observe photofluxional processes at lower temperatures than usual.

The major effect of substituting an isoelectronic first-row transition-metal ion for iron(II) is a change in the energies of the d orbitals. The consequences on the two main components of the barrier for the fluxional process are different: the interaction of the donor orbitals of pdz with the $d_{x^2-y^2}$ acceptor orbital (Figure 4) is better for the more electronegative metals, hence the contribution to the barrier due to the loss of donor–acceptor interaction increases from left to right of the periodic table. The d_{xy} orbital, on the other hand, is close in energy to the $n(b_2)$ donor and, with our current parametrization, the energy match is optimum for Fe and the four-electron repulsion contributing to the barrier increases in the order Cr < Mn < Fe > Co (Table II). One might imagine a π-bonded transition state; in a recent paper,[20] a detailed study of the geometry of the transition state has been carried out and found to be intermediate between the σ- and π-bonded structures. For our purposes, the main effect is a lowering of the calculated barriers by roughly 25%, but the qualitative trends remain unaltered.

Changes in the other ligands may also have some effect on the height of the barrier. The presence of π-acid ligands trans to the diimine results in d_{xz} being mostly localized away from the diimine while trans π-donor ligands hybridize d_{xz} toward the diimine. Hence, trans π-acid ligands should decrease and π-donor ligands increase the barrier for the haptotropic shift.

A similar analysis can be carried out for the naphthyridine octahedral complexes. Essentially, the same interactions appear but with small differences. The relative ordering of the lone pair orbitals is inverted: $n(b_2)$ has lost much of its N–N π-antibonding character as the two N atoms are taken apart, while $n(a_1)$ mixes with a σ_{CC} bonding orbital (Chart III), similarly to what happened in fmd (Figure 1), and is therefore higher in energy than in pdz. The two main components of the barrier follow the same order as for pdz, in good agreement with the available experimental data (Table II). The simplified Walsh diagram, total energy curves,

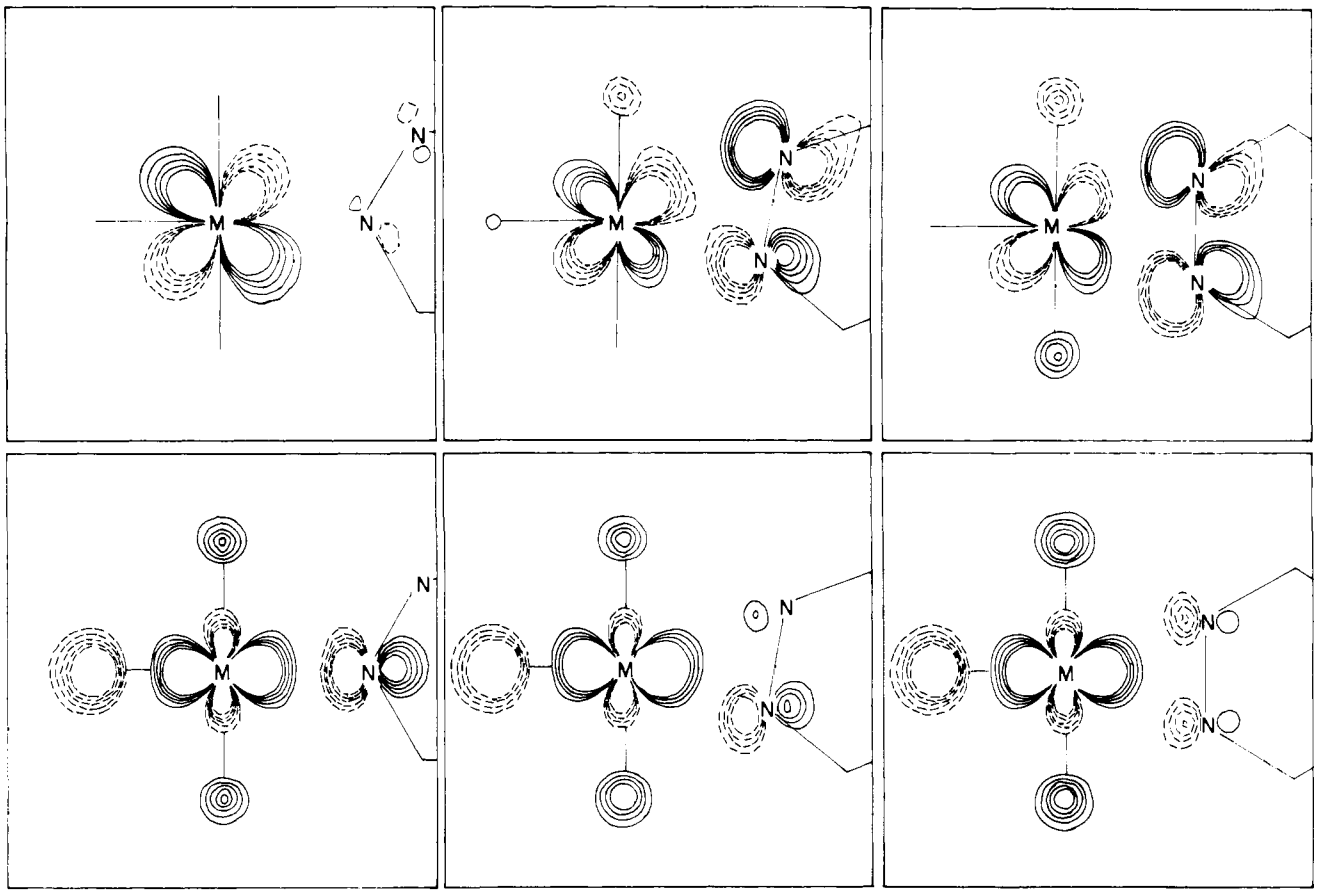

Figure 6. Contour plots of d_{xz} (above) along the monocoordinate to bicoordinate path, showing its conversion from nonbonding to antibonding through interaction with $n(b_2)$. Contour plots of the $d_{x^2-y^2}$ orbital (below) along the same path, showing the contribution of the localized $n(a_1)$ + $n(b_2)$ donor orbital in the monocoordinate case and its gradual conversion to $n(a_1)$. Mixing of d_{xz} and $d_{x^2-y^2}$ is also apparent in the intermediate step. Contours shown correspond to electron densities of 0.08, 0.10, 0.12, 0.14, and 0.16.

Scheme II

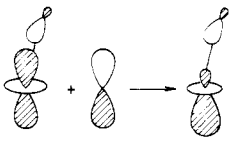

and M–N overlap populations for the iron model compounds are shown in Figure 5. The behavior of pdz and naph is qualitatively the same (Figure 5 and Table II). It has been previously suggested[6f] that differences in the lone pair orientation may account for the different barriers, but the analysis of our results indicates that the smaller N–N separation in pdz partly compensates for the worse orientation of its lone pairs.

It is worth commenting also that variations in the electronegativity of the transition metal, accomplished by artifically changing the ionization potential (H_{ii}) of the d orbitals, result in changes of the calculated barriers. Therefore, our numerical results should be taken as orientative only. This fact also suggests that changes in the set of ancillary ligands or in the metal's oxidation state should produce sizable variations of the barrier for the fluxional process.

Square-Planar Complexes

When considering the square-planar complexes, one must address first the existence of a weak axial interaction between the noncoordinated nitrogen and the metal atoms. The main orbital interaction is that of the nitrogen lone pair with d_{z^2}, a four electron–two orbital destabilizing one. Mixing of p_z diminishes the antibonding character of d_{z^2} as schematically shown in Scheme II, hence accounting for the weak axial interaction, as shown in our calculations for $[M(PH_3)_2Cl(naph)]^+$ (M = Ni, Pt) by both a positive $M-N_{ax}$ overlap population and the occupation of the metal p_z orbital by 0.15 e. However, the axial bonding situation

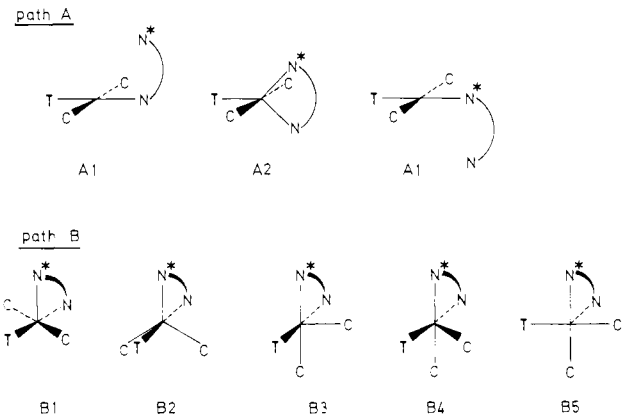

Figure 7. Sliding (A) and pseudorotation (B) pathways for the haptotropic shift in square-planar complexes.

appears to be energetically unfavorable, probably due to an exageration of four electron interactions in Extended Hückel calculations, making direct comparison of energies for different geometries in these complexes a delicate matter. Additionally, when the diimine is pyridazine, the axial interaction appears to be worse than for naphtyridine because that ligand is not able to occupy an axial coordination position without a sensible loss of equatorial overlap.

The main difference between square-planar ML_3 and octahedral ML_5 fragments is that alternative mechanisms are available in the former case. One is a sliding motion similar to the one used for octahedral fragments (path A in Figure 7), in which the intermediate is a trigonal bipyramid (TBP) with both N atoms occupying equatorial positions and the ligands retain their cis or trans positions. Another possible pathway is a Berry pseudorotation[21] (path B in Figure 7), passing through TBP and square-

Chart IV

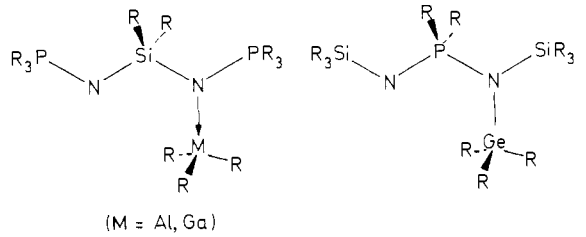

pyramidal (SP) intermediates; these trigonal bipyramids have one N atom in an axial and one in an equatorial position. Cis and trans ligands exchange their positions along this path.

Let us comment first on the sliding pathway discussed above for the octahedral fragments, assuming no axial interaction to begin with, due to the methodological limitations stressed above. The orbitals of an ML_3 SP fragment resemble those of the ML_5 octahedral one, except for the d_{z^2} orbital, which is now nonbonding and occupied. The essentials of the orbital interactions between an ML_3 group and the ligand in both the mono- and bidentate situations are therefore coincident with those found for ML_5. The factors controlling the height of the potential energy barriers are expected to be the same as previously found for octahedral complexes. Some calculated barriers for this mechanism are collected in Table II. An interesting result is the barrier lowering upon substitution of the carbon atom in the formamidinate ligand (fmd) by a nitrogen in triazenido (tzd), similar to that predicted above for the proton shift, and consistent with the experimental figures for the corresponding Pd and Pt complexes (Table II).

Notice that through the pathway discussed so far (path A in Figure 7) the *cis*-phosphine ligands always remain cis, but at least in one case[6g] the changes in the NMR spectra with the temperature indicate interconversion of *cis*- and *trans*-phosphines. This fact is compatible with a dissociative mechanism, but also with a Berry pseudorotation mechanism (path B in Figure 7).

By looking at the two types of intermediates B2 and B3 we can get a qualitative idea of how good the pseudorotation path is. The trigonal-bipyramidal intermediate B2 is similar in energy to the A2 bipyramid for both pyridazine and naphtyridine. Evolution to the square-pyramid B3 should not require much activation for a general pentacoordinate species.[22] However, the bidentate nature of the ligands under investigation imposes geometrical constraints which make the energy of the B3 intermediate higher than expected. Although full geometrical optimization might lower the calculated barriers, these results probably indicate that this pathway is much more energetic than the sliding mechanism for both pdz and naph.

Main Group Elements

Fluxional compounds with related ligands have been reported for Al, Ga, and In;[11] Si and Ge;[12] and P.[25] The ligands reported to undergo fluxional behavior are saturated in all these cases (Chart IV), but the topology of the lone pairs involved is similar to those of the formamidinate or naphtyridine ligands (Chart I). It is interesting to study these compounds in search of similarities and differences with transition-metal complexes.

Calculations for a model compound of Al and naphtyridine, H_3Al(naph), give an estimated barrier of 7 kcal/mol for the haptotropic shift, sensitively smaller than those calculated for the transition-metal complexes. We can conclude that main group metals should always produce smaller barriers than transition metals with the same ligand. There are two good reasons for this behavior: (a) The only metal orbitals of π character with respect to the M–N bond for the non-transition metals are the pair of e orbitals (p_x and p_y), of M–H bonding character and too low in energy to interact with $n(b_2)$ in the bidentate transition state, thus avoiding the four-electron repulsion commented on above for the transition metals. (b) The loss of overlap between the N-donor orbitals and the metal a_1 acceptor, on going from a mono- to a bidentate situation, is significantly smaller for a main group metal (Table III). The interaction of the $n(b_2)$ lone pair with the metal a_1 orbital falls to zero for the bidentate case in both the Fe and the Al complexes, and only a residual overlap with the H atoms attached to Al remains. The interaction of $n(a_1)$ with the metal a_1 orbital decreases for the transition metal but is practically constant for the main group metal. The different behavior of this

Table III. Overlap Integrals between the a_1 Acceptor Orbitals of Metal Fragments and the Two Lone Pair Orbitals of Pyridazine, $n(a_1)$ and $n(b_2)$

		CrH_5	AlH_5
b_2	monodentate	0.123	0.098
	bidentate	0.000	−0.007
a_1	monodentate	0.148	0.137
	bidentate	0.099	0.133

Table IV. Orbital Exponents (Contraction Coefficeints of Double-ζ Expansion Given in Parentheses) and Energies Used in the Calculations

atom	orbital	ζ_μ	ζ_μ'	$H_{\mu\mu}$ (eV)
C	2s	1.625		−21.4
	2p	1.625		−11.4
N	2s	1.950		−26.0
	2p	1.950		−13.4
H	1s	1.3		−13.6
Cr	4s	1.70		−8.66
	4p	1.70		−5.24
	3d	4.95 (0.4876)	1.60 (0.7205)	−11.0
Mn	4s	1.80		−9.75
	4p	1.80		−5.89
	3d	5.15 (0.5140)	1.70 (0.6930)	−11.67
Fe	4s	1.90		−9.10
	4p	1.90		−5.32
	3d	5.35 (0.5366)	1.80 (0.6678)	−12.60
Co	4s	2.00		−9.21
	4p	2.00		−5.29
	3d	5.55 (0.5550)	1.90 (0.6460)	−13.18
Ni	4s	2.10		−10.95
	4p	2.10		−6.27
	3d	5.75 (0.5683)	2.00 (0.6292)	−14.20
Pd	5s	2.19		−7.32
	5p	2.152		−3.75
	4d	5.983 (0.5264)	2.613 (0.6733)	−12.02
Pt	6s	2.554		−9.077
	6p	2.535		−5.475
	5d	6.013 (0.6331)	2.696 (0.5516)	−12.59

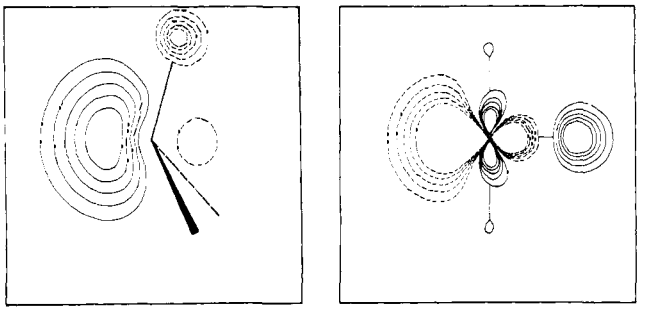

Figure 8. Contour plots for the a_1 acceptor orbitals of CrH_5^{2-} (left) and AlH_3 (right), clearly showing the wider shape of the latter due to its larger s contribution. Contours shown correspond to electron densities of 0.05, 0.07, 0.09, 0.11, and 0.13.

(21) For a recent review on the mechanisms of substitution reactions on square-planar complexes, see: Cross, R. J. *Chem. Soc. Rev.* **1985**, *14*, 197.

(22) According to the Angular Overlap Model, a square pyramid for a d^8 metal should be slightly more stable than a trigonal bipyramid (Burdett, J. K. *Molecular Shapes*; J. Wiley: New York, 1980; p 189). Taking experimental Angular Overlap parameters for Ni from ref 23, the difference in energy can be estimated to be of about 6 kcal/mol. For an analysis of the pseudorotation problem, see also ref 24.

(23) Lever, A. B. P. *Inorganic Electron Spectroscopy*, 2nd. ed.; Elsevier: New York, 1984.

(24) Rossi, A. R.; Hoffmann, R. *Inorg. Chem.* **1975**, *14*, 365.

(25) (a) Winkler, T.; Philipsborn, W. V.; Stroh, J.; Zbiral, E. *J. Chem. Soc., Chem. Commun.* **1970**, 1645. (b) Scherer, O. J.; Schmitt, R. *J. Organomet. Chem.* **1969**, *16*, P11. (c) Scherer, O. J.; Hornig, P. *Chem. Ber.* **1968**, *101*, 2533.

overlap can be attributed to the difference in hybridization of the metal a_1 orbital: it is a dsp hybrid in the transition metal, with only 5% s character in the octahedral fragment and 4% s character in a square-planar fragment, but an sp hybrid in the main group metal (Al), with 25% s character. The larger s contribution makes the orbital more diffuse for Al (see contour plots in Figure 8), thus avoiding important loss of overlap upon ligand sliding.

Unfortunately, systems with the same ligand for both a transition metal and a main group element have not been studied so far and our comparison cannot be carried on to the experimental data. Let us remark, however, that the calculated barriers for the pdz and naph derivatives are practically identical (Table II), at difference with the results for the analogous derivatives of transition metals. Since the b_2 component of the barrier is negligible for the main group metals, these results confirm our previous assertion that the major difference between both ligands corresponds to their different b_2 repulsions at the bidentate transition state, but not to differences in the loss of a_1 overlap.

Appendix. Computational Details

All calculations were of the Extended Hückel type[26] with modified Wolfsberg-Helmholtz formula.[27] The parameters used were taken from the literature[28] and are collected in Table IV. Calculations were carried out on the following model compounds: fmd^-, fmdH, tzd^-, tzdH, $[CrH_5L]^{5-}$, $[MnH_5L]^{4-}$, $[FeH_5L]^{3-}$, $[FeCp(CO)_2L]^+$, $[PtCl(PH_3)_2(fmd)]$, $[PtCl(PH_3)_2(tzd)]$, $[MCl(PH_3)_2L]^+$ (L = pdz, naph; M = Ni, Pd, Pt). The experimental geometry[5a] was used for fmd and Pt-fmd and kept the same for tzd. Idealized geometries were used for the aromatic ligands pdz and naph, taking all ring distances equal to 1.40 Å, C-H distances of 1.08 Å, and bond angles of 120°. M-N distances were taken as 2.10 Å, a representative value for most of the studied complexes; also frozen representative distances were used for other metal-ligand bonds: M-Cl = 2.20, M-P = 2.20, M-H = 1.75 Å.[5,6,29]

Acknowledgment. The computational part of this work was supported by CAICYT through Grant No. 0657/81. We are indebted to Profs. J. Strähle and T. A. Albright for providing us with their results prior to publication.

(26) Hoffmann, R.; Lipscomb, W. N. *J. Chem. Phys.* **1962**, *36*, 2179, 3469; **1962**, *37*, 2872. Hoffmann, R. *J. Chem. Phys.* **1963**, *39*, 1397.

(27) Ammeter, J.; Bürgi, H.-B.; Thibeault, J.; Hoffmann, R. *J. Am. Chem. Soc.* **1978**, *100*, 3686.

(28) Alvarez, S. *Table of Parameters for Extended Hückel Calculations*; Universitat de Barcelona: Barcelona, 1985.

(29) Teller, R. G.; Bau, R. *Struct. Bond.* **1981**, *44*, 1.

Spin-Orbit Coupling in Biradicals. Ab Initio MCSCF Calculations on Trimethylene and the Methyl-Methyl Radical Pair

Louis Carlacci,[†] Charles Doubleday, Jr.,*[‡] Thomas R. Furlani,[⊥] Harry F. King,*[†] and James W. McIver, Jr.*[†,∥]

Contribution from the Department of Chemistry, State University of New York at Buffalo, Buffalo, New York 14214, Chemistry Department, Columbia University, New York, New York 10027, Calspan Advanced Technology Center, Buffalo, New York 14225, and Department of Chemistry, Canisius College, Buffalo, New York 14208.
Received January 20, 1987

Abstract: Spin-orbit coupling (SOC) constants are computed by ab initio MCSCF (multiconfiguration self-consistent field) theory for the trimethylene biradical, $^{\bullet}CH_2CH_2CH_2^{\bullet}$, and for a pair of interacting methyl radicals as functions of separation and relative orientation of radical centers. The effects of through-bond coupling are analyzed by comparing SOC values for the biradical with those for a radical pair with the same orientation of $^{\bullet}CH_2$ centers. Ab initio results for the radical pair are found to be well-described by the semiempirical formula, SOC = $B|S|\sin\phi$, where ϕ is the acute angle between radical p orbitals, S is the orbital overlap integral, and B = 15 cm^{-1}. Predicted values require correction by a factor of 3.0 or less in the event of strong steric interaction with a radical p orbital. The principal effect of through-bond coupling by a single CH_2 moiety is to increase SOC by another factor of about 2.5. We discuss the implications of these computational results for the interpretation of recently measured rate constants for intersystem crossing in a 1,3- and a 1,4-biradical system. We conclude that the slower rate in the 1,3-biradical is due to the Boltzmann factor associated with the activation energy required to reach the singlet-triplet crossing.

A major challenge in the chemistry of organic biradicals and radical pairs is the problem of treating intersystem crossing (ISC) between singlet and triplet states. The problem is important because biradicals generated from triplet precursors must first undergo ISC before products can be formed. Thus, ISC influences both the rate of product formation[1] and the product ratio.[2] Scheme I presents a general kinetic model that has proved useful for interpreting experimental results. Three categories of kinetic processes are important: (1) ISC; (2) chain dynamics in the case of biradicals or diffusive displacements in the case of radical pairs in solution; (3) the product-forming step, typically a process on the singlet surface.

[†] State University of New York at Buffalo.
[‡] Columbia University.
[⊥] Calspan Advanced Technology Center.
[∥] Canisius College.

(1) (a) Zimmt, M. B.; Doubleday, C. Jr.; Turro, N. J. *J. Am. Chem. Soc.* **1986**, *108*, 3618-3620. (b) Caldwell, R. A. *Pure Appl. Chem.* **1984**, *56*, 1167-1177. (c) Scaiano, J. C. *Acc. Chem. Res.* **1982**, *15*, 252-258. (d) Closs, G. L.; Miller, R. J.; Redwine, O. D. *Ibid.* **1985**, *18*, 196-202.

(2) (a) Doubleday, C., Jr. *Chem. Phys. Lett.* **1979**, *64*, 67-70. (b) Doubleday, C., Jr. *Chem. Phys. Lett.* **1981**, *79*, 375-380. (c) Caldwell, R. A.; Creed, D. *J. Phys. Chem.* **1978**, *82*, 2644-2652. (d) Scaiano, J. C.; Lee, C. W. B.; Chow, Y. L.; Marciniak, B. *Ibid.* **1982**, *86*, 2452-2455. (e) Scaiano, J. C. *Tetrahedron* **1982**, *38*, 819-824.

0002-7863/87/1509-5323$01.50/0